Bubble property determination.

Comparison between bubble data from a fibre probe, and a camera.

by

Jille van der Bom

Student Name	Student Number Delft	Student Number Leiden
E.J. van der Bom	4726979	s2718545

daily supervisor:	Rik Volger
Supervisor:	dr. ir. Cees Haringa
2nd Examiner:	dr. Adrie J.J. Straathof
Project Duration:	April, 2023 - July, 2023
Faculty:	Faculty of Applied Sciences, Delft

Abstract

An optical fibre probe was tested in liquids with biotechnologically relevant compounds, to determine if any limits arise in bubble property determination due to these compounds. The data from this fibre probe was compared to the data from a camera for which an image processing algorithm was developed. This algorithm was able to successfully filter objects using configurable parameters. Objects had to be in focus, within a certain size range and elliptical in shape. The filtering was able to work with partially out of focus bubbles, and bubbles at the edges of the image within tolerances specified by the parameters. To provide insight into the relation between the fibre probe data and camera data a control measurement was performed in pure water, after which measurements were performed in a mixture containing 100g/L ethanol and a mixture containing 0.4M NaCl. The data sets from both measurement methods were compared for bubble velocity and bubble size. The velocity would be directly comparable, the size was however the local height at the point where the fibre probe pierced the bubbles. As such the height directly below the fibre probe of the bubbles was determined from the images to serve as comparable data. The comparison between the probe data and camera data was inconclusive due to a dissimilarity between the distributions. Mainly the overestimation of the comparable size from the camera data was a problem. Which was likely due to the camera showing only a 2D projection of the bubble and as such the entire height would be used for this comparison. For the velocity the camera data had a narrower distribution as compared to the fibre probe data. This could be caused by the camera averaging the speed of bubbles between two or even three frames if a bubble was not detected in the middle frame, the probe might be more sensitive to these variations and as such yield a wider distribution. The image processing algorithm showed a correct processing of the images to yield usable data, the exact comparable data however still needs to be improved for this specific application.

Contents

1 Introduction

To transition to a more biobased society a lot of conventionally (petro)chemical processes will need biochemical alternatives. To be economically viable and competitive with the traditional processes, efficiencies and process speeds need to increase. Improving these factors requires correct predictive models, for example computational fluid dynamics (CFD) models, which require data to base the interactions on. One of the most important interactions is between different phases, which can determine (limiting) mass and energy transfer rates. Bubble properties are one of the factors with the greatest variation and largest effect on mass transfer rates in gas-liquid phase processes. Bubble properties can influence the gas holdup and the specific interfacial area (Garcia-Ochoa and Gomez, 2009). In processes where a transfer from the gas to the liquid is required, this transfer is often a limiting factor. The volumetric mass transfer coefficient is the product of the specific interfacial area (a) between the gas and the liquid and the mass transfer coefficient (k_L). As such by increasing the specific interfacial area the mass transfer will also be increased. Bubble size distribution is one of the main factors influencing this aspect of mass transfer. The shape of bubble size distributions have been hypothesized to follow a lognormal distribution (Besagni and Inzoli, 2016), however these are still assumptions (Augier and Raimundo, 2021).

An important aspect of comparing non spherical bubbles is the equivalent diameter. Bubbles can be perfectly spherical, this is however unlikely, and they are often more elliptical in shape. Compare bubble sizes an equivalent diameter is often used which is the diameter of a sphere with the same volume as the ellipse. This eliminates the difference between the major and minor axis of the elliptical bubbles. Following this the equivalent diameter (d_e) (with a the major axis, and b the minor axis) is calculated as follows:

$$d_e = (a^2 * b)^{1/3}$$

Measuring bubble properties has a lot of challenges, and as such each method has it's drawbacks and advantages. One method is using a camera for visualization, this is possible up to a certain gas hold-up (Colombet et al., 2011). In biotechnological processes there is usually a higher gas-holdup, and moderate gas-holdup already makes image processing more difficult. This is due to distortion or obstruction of in focus bubbles by other bubbles. Additionally in biotechnological processes the fluid is usually opaque due to cells and other compounds, and as such visually inaccessible. Studying bubbles in water-air systems can provide insights into the bubble properties, however a large amount of compounds present in biotechnological processes have an effect on these properties (Keitel and Onken, 1982). Thus using a water-air model to predict bubble and mass transfer properties could yield incorrect results, as shown by Puiman et al. (2022). A different method of measuring bubble size and speed is through optical fibre probes, one end is submerged in the liquid, the other end has a optic sensor and laser. By measuring the internal refraction(fig 1.1) the phase at the fibre tip can be determined because refraction in air is at least tenfold higher than in water (Lefebvre et al., 2022).

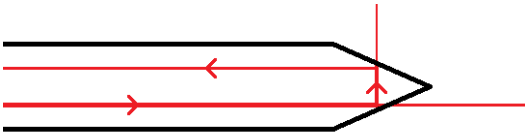

Figure 1.1: Schematic illustration of the fibre probe tip with edges in black, laser in red. Thinning of the lines illustrates decreased intensity. (angles and sizes not to scale)

By using multiple of these probes (W. Bai et al., n.d.) the speed of bubbles can be determined, combining the speed with the gas duration at the tips results in the height of these bubbles. This method has some drawbacks, the bubble has already interacted with the first tip when arriving at the second tip, and as such their speed and shape could have been influenced by this contact. Furthermore the distance between the tips creates a lower limit for the minimal bubble diameter which can be measured. To limit the effects of this interaction Lefebvre et al. (2022) proposed an improved fibre probe by using the shift of interference between the internally reflected signal and the signal reflected of a (bubble) interface to determine the speed of the approaching interface. This removes the limitation of a minimal bubble diameter due to the separation between the tips, and also removes a lot of uncertainty caused by the direction of bubble movement. Such probes have been used in the past but weren't very common due to limited availability of sufficiently fast and large converters. This fibre probe can give very precise local measurements of bubble velocity and size, and gas hold-up (Lefebvre et al., 2022) even in visually inaccessible liquids. This could make it a suitable measurement device in biotechnological processes. One drawback is however the size it measures is the height of the bubble at the point where it pierces the bubble, which makes the data not directly comparable with other measurement techniques, and unsuitable for constructing correct models.

However the compounds in biotechnological processes that influence the bubble properties could also influence the interaction between a bubble and the probe. Salts and alcohols are among the compounds that have an influence on the bubble properties, this happens through a multitude of effects. One of these effects is decreasing the rate of coalescence, coalescence is the process where two colliding bubbles merge to form one larger bubble. The relationship between salt concentration and bubble size shows a sharp decrease in bubble size around a specific concentration, the so-called transition concentration. This transition concentration is unique to each salt and exact values vary based on measurement conditions (Firouzi et al., 2015). For NaCl this transition concentration lays in between 0.1M and 0.3M (fig 1.2) depending on the measurement method used and the exact definition for the transition concentration, all clear transitions are however smaller than the total range.

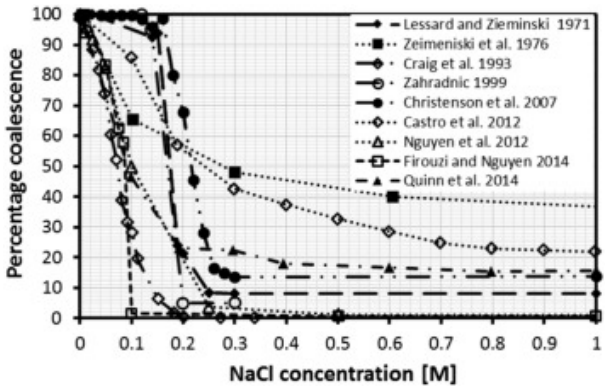

Figure 1.2: Comparison between different determinations of the percentage coalescence in NaCl solutions as performed by Firouzi et al. (2015)

Alcohols among other organic compounds show a decrease in coalescence with increasing concentrations, and again the exact relation between the concentration and bubble size is dependent on the exact alcohol present (Keitel and Onken, 1982). For alcohols the effect is spread over a larger concentration range, a concentration of 1 g/L ethanol already shows an effect on bubble size, and at concentrations of 10g/L there is still an increase of specific interfacial area (Keitel and Onken, 1982). CO-fermentation

processes which produce ethanol can contain concentrations up to 48g/L (Klasson et al., 1993), for other ethanol fermentation processes this can be upwards of 10-12% (v/v) which is around 80-95g/L (F. W. Bai et al., 2008), and growth and ethanol production inhibition occurs mainly above 100g/L (Luong, 1985). The solutes that act as surfactants could also reduce single bubble velocity, this is due to increased friction imposed on the bubbles in liquids with surface contaminants. This is partially caused by the bubbles acting more like rigid bodies (Park et al., 2017). The solutes with the most significant influence on the drag coefficient and gas holdup are amphiphilic (both hydrophobic and hydrophilic), which causes them to be mainly present at the gas-liquid interface (McClure et al., 2014).

Both coalescence inhibition and the bubbles acting more like rigid bodies are factors that might affect the interaction with the fibre probe, and decreasing the chances of the probe successfully piercing the bubbles. This decrease might be equal for all bubbles or it might depend on the velocity, size or both. If less bubbles are pierced overall the gas hold-up could be estimated incorrectly. If there are bubbles with specific properties which are pierced significantly less than others then the distributions shown by the probe could be skewed. Usage of these distributions can lead to incorrect calibration of CFD models, or over- or underestimation of the available area for mass transfer. To determine if such limits occur in biotechnologically relevant fluids a validation should be performed where the data of the fibre probe is compared to data of a different measurement method of which the limits are known. As long as the conditions allow the measured bubbles to be visually accessible this method could be a camera pointed at the fibre probe. By testing the fibre probe and a camera simultaneously with known concentrations of a single solute, the effect of this solute on the fibre probe data could be determined. In this report the results of an attempt at such a validation are shown for NaCl and Ethanol at concentrations certain to have an effect on the bubble properties. Measuring at the extremes shows if these compounds induce any limits in the measurements of the probe, and if not, no limits would be expected at lower concentrations either. Thus for NaCl a concentration above the found transition concentrations, of 0.4M will be used. For ethanol the concentration around where growth inhibition starts to occur, of 100 g/L will be used. The possible limits of the fibre probe and their implications resulting from the addition of these compounds are then discussed.

List of Symbols

Symbol	Unit	Description
a	m^2/m^3	specific interfacial area
d_e	m	(volume) equivalent diameter
g	m/s^2	gravitational acceleration
k_L	m/h	mass transfer coefficient
M	mol/L	Molarity of a solution
Q_{vd}	s^{-1}	velocity bubble diameter limit ratio
v	m/s	velocity
v_b		expected terminal bubble velocity based on diameter
$v_{b,vis}$		expected velocity when inertial forces are negligible compared to viscous forces for spherical bubbles.
$v_{b,in}$		expected velocity for spherical bubbles with nonnegligible inertial forces.
$v_{b,spheroid}$		expected velocity for spheroidal bubbles.
v_max		maximum detectable rise velocity
μ_L	Pa*s	Viscosity of a liquid
ρ_L	Kg/m^3	Liquid density
σ_L	N/m	surface tension of the liquid

2

Technical Background

2.1. Bubble imaging

The method used to determine bubble properties was a camera in combination with a bubble determination algorithm which combined several methods of imaging processing to determine both the size and velocity of the bubbles. To determine the settings and from these the limitations of the camera setup, several calculations are required. These calculations have input values for camera settings (FPS, shutter speed), lens properties (aperture and focal length) and physical constraints (preferred field of view, length of the fibre probe in view). Several considerations will have to be made concerning these input values. For the FPS an as high as possible value will be preferred, this would reduce the height of the field of view necessary to determine the bubble rise velocity. Because the amount of pixels is limited, a smaller field of view will yield a higher precision, which is preferred. Because at least two images of the bubble are necessary to calculate the speed, the maximum measurable rise velocity can be calculated as follows:

$$v_{max} = \frac{FOV_{effective} * FPS}{2}$$

The effective field of view ($FOV_effective$) is equal to the part of the image without the fibre probe in view, because the fibre probe slows down bubbles (Lefebvre et al., 2022), velocity can only be properly determined for bubbles free from the probe. The length of the fibre probe in view will have to be minimal, to increase the effective area for the velocity measurement. However the fibre probe has to be in view to assure the bubbles in view are share their properties with the bubbles measured by the probe, this will also allow the fibre probe to be used as a size reference. The camera and fibre probe will be aligned horizontally and the fibre probe will be lowered into view (fig 2.1).

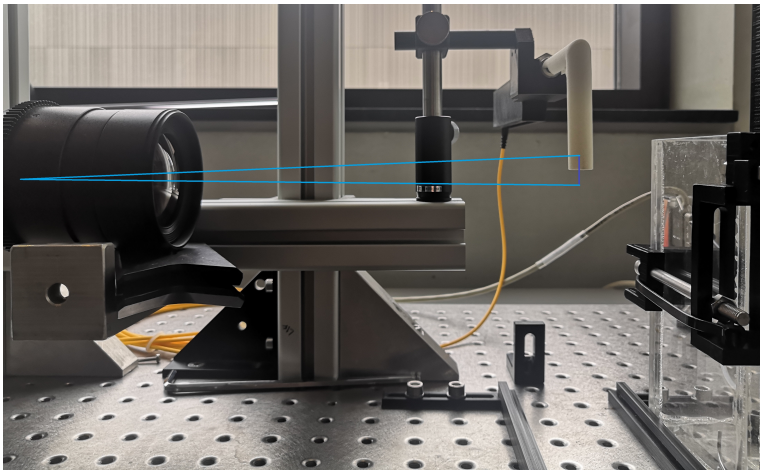

Figure 2.1: Image of the camera and fibre probe (with protective white cap) with line drawn to illustrate field of view (dark blue), and outer sight lines (light blue). Lines not to scale.

To keep blurring of the image to a minimum exposure time (shutter speed) will be minimized, it is preferable to keep the error caused in the size determination by this blurring to less than 5% of the bubble size. From the shutter speed a limit ratio between the bubble velocity and size can be determined.

$$Q_{vd} = \frac{blurringFraction}{shutterspeed \times 10^3} \tag{2.1}$$

With the percentage for blurring as a fraction and the shutter speed multiplied by 10^3 for the correct magnitude.

$$v(m/s) = Q_{vd} \times d(mm) \tag{2.2}$$

Comparing this limit to the formula (2.3) constructed by Park et al., 2017 will show if it is to be expected if a part of the expected bubbles will cross this limit.

$$v_\mathrm{b} = \frac{1}{\sqrt{\frac{1}{v_{\mathrm{b,vis}}^2} + \frac{1}{v_{\mathrm{b,in}}^2} + \frac{1}{v_{\mathrm{b,spheroid}}^2}}} = \frac{1}{\sqrt{\frac{144\mu_\mathrm{L}^2}{g^2\rho_\mathrm{L}^2 d_\mathrm{e}^4} + \frac{\mu_\mathrm{L}^{4/3}}{0.14425^2 g^{5/3}\rho_\mathrm{L}^{4/3} d_e^3} + \frac{1}{\frac{2.14\sigma_\mathrm{L}}{\rho_\mathrm{L} d_\mathrm{e}} + 0.505 g d_\mathrm{e}}}}. \tag{2.3}$$

To create a realistic physical setup of the column with the probe, along with the camera and the lens, a macro lens will be preferred. Macro lenses have a longer focus distance and a more narrow field of view. These properties allow a small field of view around the probe, with the camera outside of the column. The aperture will be minimal to decrease the depth of view, this ensures only bubbles close to the probe will be pictured clearly with sharp edges.

2.2. Image processing

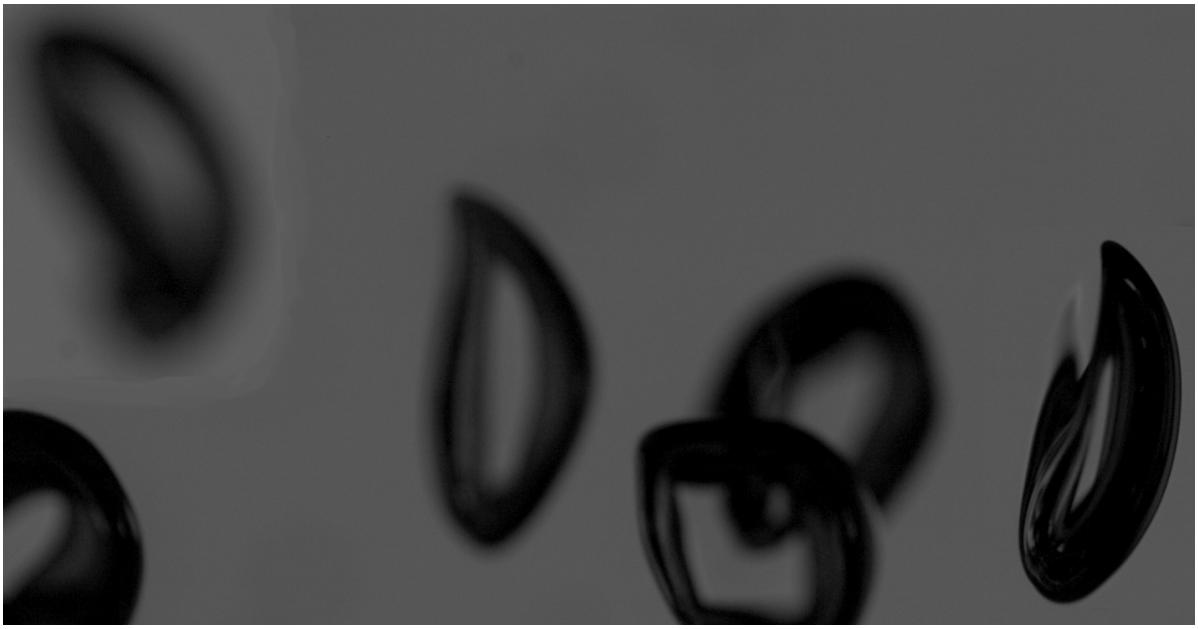

Figure 2.2: Artificially constructed image showing several bubbles to demonstrate the different filtering aspects of the algorithm. left bottom shows a sharp bubble largely of the image, top left shows a very out of focus bubble, middle center show a just out of focus bubble, right center shows two overlapping bubbles, bottom right shows an in focus bubble.

For the image processing a piece of software is required to determine what objects on the image were usable bubbles. A few selection criteria would need to be passed by an object to yield usable data for a comparison with the fibre probe data. The bubbles would need to be in focus to ensure proper size estimation, they would need to be single bubbles, and have a sufficiently large part visible on the image for bubbles at the edges. Several processing algorithms exist and are discussed in papers (Colombet et al., 2011)(Zhou and Niu, 2020). The actual source code is however very difficult to find, and not all

properties were directly applicable to this project. As such an algorithm was created using Python, utilizing several public libraries. The first version of the algorithm used the library Trackpy ("Python code for bubble tracking", n.d.) and some sample code to track movement in bubble foams. This allowed the tracking of bubbles in a dense foam, however the determination of which objects were actual bubbles was very crude. To further refine this part of the processing inspiration was taken from Villegas et al. (2019).

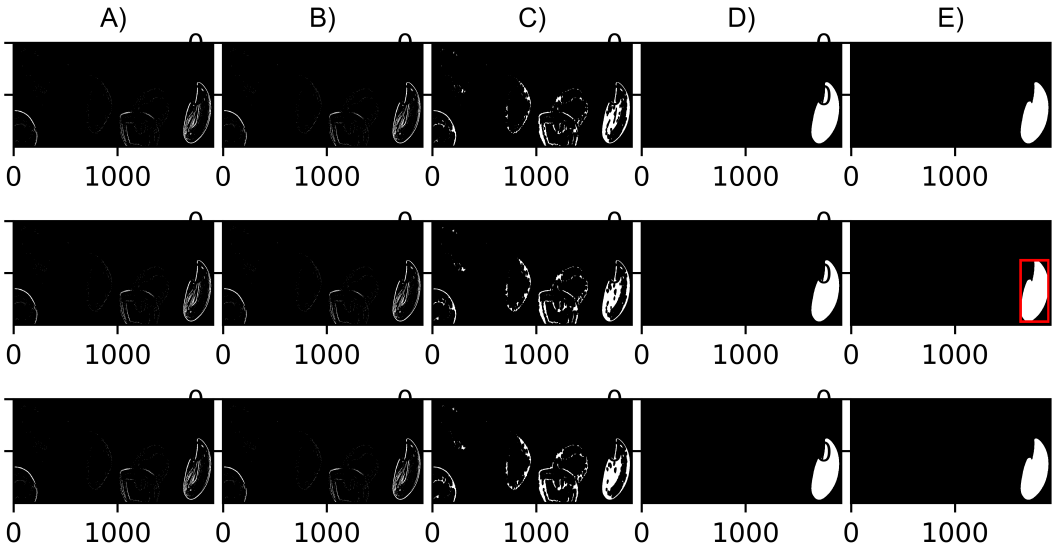

Figure 2.3: Images of the different configurable processing steps performed by the algorithm. The image used is an artificial composition of several bubbles to show the effects of different bubbles. Columns show the steps as follows: A) Sobel threshold, B) Edge closing maximum distance, C) Closing ellipse kernel size, D) Minimal object area, E) Fraction of object in ellipse. The red box is the bounding box for the recognised object.

To show the operation of the algorithm an artificially constructed image was used (fig 2.2) which had different types of bubbles which could be expected to show all aspects of the filter. First the algorithm would discard the bubbles which were out of focus, for this a Sobel-Feldman operator was used (fig 2.3A), this changes the intensity of pixels based on the difference in intensity with neighbouring pixels, yielding a grey scale image with lighter pixels representing in focus edges of objects. Filtering only the pixels above a certain threshold leaves only in focus edges in the image. The edges of the bubbles connecting to the edge of the image are closed (fig 2.3B) if the stretches of black pixels are small (within a single bubble), this ensures the image edge will be seen as part of the outermost edge in the second to last step. Then using morphological operations the outlines of the bubbles within the image are connected using an elliptical kernel ("OpenCV: Morphological Transformations", n.d.) this elliptical kernel will have to be similar in shape and orientation as the bubbles, but a lot smaller(fig 2.3C). This operation ensures objects with a similar shape to the general bubbles will be favored during processing. Following this only the largest edge of a series of nested edges is kept, this discards any areas still inside bubbles. The edges are stored as a set of coordinates within the image, an ellipse is then fitted over this shape to determine if the bubble can be represented by an ellipse (fig 2.3D). To fit the ellipse an existing Python method (Christian, 2021) was used. If the ellipse and the bubble have enough overlap, and the bubble is large enough (fig 2.3E)then the bubble shape is drawn on the image, and the ellipse properties are stored to determine the equivalent diameter. The exact values for all the settings depend on the image size and bubble properties as such these settings will be determined iteratively using the results from the experiments. The cross-sectional area on the height of the probe in the image is used as a comparable diameter for the diameters measured by the probe. This accounts for off-center piercing by the probe. The processed images are then used to track the bubbles and extract their velocities from the trajectories. The camera data can then be compared to the probe data, and possibly a

relationship between the diameter as measured by the probe and the equivalent diameter determined by the algorithm can be estimated.

2.3. Measurements

To ensure the measurements will be representative of the actual values the measured mean should approach the actual mean. For this a sufficiently large sample size is necessary, to determine this sample size, we can use the relationship (2.4 constructed by Hale (1972). Which gives the required sample size (n) using a specified confidence level (Z), the standard deviation of the logarithms of the observations (S), and the fraction of the observed geometric mean by which it can differ from the true geometric mean (P). This means that for a 95% confidence level (Z=1.96) the geometric mean from the measurements will deviate from the true mean at most by fraction P in 95% of all cases.

$$n = \frac{Z^2 S^2}{ln^2(P+1)} \tag{2.4}$$

To determine if the data sets are (log)normally distributed a shapiro test or 1 sample Kolmogorov-Smirnof test (KS-test) can be performed, the first is suited to samples with n<50. As such the latter will be performed, this test assumes the data is (log)normally distributed and this hypothesis can be rejected if the p-value is lower than 0.05. Normally distributed data will be compared using two sample t-test. A KS-test can be used in all other cases to test if the distribution of both is similar. If the p-value of these tests is below 0.05 we can reject the null hypothesis, which states that these distributions are similar. For the t-test this shows their means do not differ significantly and for the KS-test this shows that these data sets come from the same distribution.

3

Materials & Methods

3.1. Fibre Probe and Column

The fibre probe used was a "M2 Bubbly Flow Analyzer" build by A2 Photonic Sensors. The probe would be suspended in a custom build column made from acrylic with inner dimension of 145mm(height), 80mm(width), 50mm(depth). The bubble probe will be at least 10-20mm below the fluid surface to ensure bubbles floating on the liquid surface would not interfere with bubbles flowing past the probe. The probe will be as high as possible to allow the bubble velocity to approach terminal velocity as close as possible. The gas used will be N_2 the flow will be controlled by a Bronkhorst flow controller with a maximum flow of 5 L/min (N_2. The pressure supplied was around 0.2 bar which allows in the flow controller being able to supply a gas flow of 0.027-0.031 L/min, which was the lowest possible flow. The gas inlet used was a capillary tube with an 1/16 inch (1.5875mm) outer diameter and a 0.03 inch (0.762mm) inner diameter of 20 cm long. The glass fibre tip of the probe was 125μm thick.

3.2. Camera

For this experiment an "acA1920-150uc - Basler ace" camera (AG, n.d.) was used. This camera had a maximum FPS of 150, and a minimal shutter speed of 105 μs. To determine the preferred field of view a length of 2 mm of the probe was chosen to be in view, along with the expected maximum velocity of 0.45 m/s (Park et al., 2017) resulted in a field of view with a height of 15 mm. with the camera on its right side to have the most pixels available in the vertical direction, this means all bubbles moving up will be seen as moving from right to left. with 1920 pixels on the sensor of this camera a pixel would represent around 7.8 μm, at which scale the probe will be 16 pixels wide in the image. With the shutter speed at the lowest value, blurring due to the speed of the bubbles would be minimised. To ensure blurring of the edge does not exceed 5% of the total bubble size, the formula for the limit ratio between velocity (m/s) and size (mm) (eq 2.1) can be applied with the minimal shutter speed of the used camera, which yields:

$$Q_{vd} = \frac{0.05}{105 * 10^{-6} s \times 10^3} = 0.476 s^{-1} \tag{3.1}$$

The formula for the velocity limit (eq 2.2) becomes:

$$v(m/s) = Q_{vd} \times d(mm) = 0.476 \times d(mm) \tag{3.2}$$

Comparing this limit to the parametrization as constructed by Park et al., 2017 shows (fig 3.1) it can be assumed this limit will be reached only rarely.

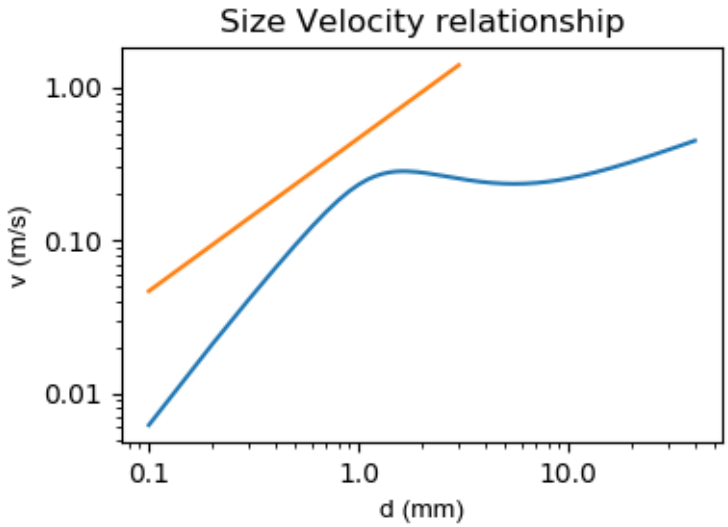

Figure 3.1: A comparison between the limit at which motion blur of a bubble is equal to 5% of it's size (in orange) and the estimated values for bubble rise velocity (m/s) for a given diameter (mm) (in blue). The limit velocity is always higher than the expected velocity which means any motion blur will be below 5% of a bubbles size.

Other properties for the camera were chosen to provide a clear picture with enough lighting. A macro lens with a focal length of 100 mm was used, and a focus distance of 259 mm would be necessary to yield the preferred field of view. The aperture was set to 3.1 as this was the lowest possible value for this lens, and the focus was tuned to yield a sharp image (3.2) of the probe which resulted in a focus distance of 370-380 mm, with the back of the camera 415 mm from the probe it is reasonable to assume these values line up. Lastly the ISO value could not be controlled as such, the used camera had a gain value for the signal. The gain was set to 0 dB because the lighting proved enough to yield a good contrast in the picture, and a higher value would increase noise in the camera signal.

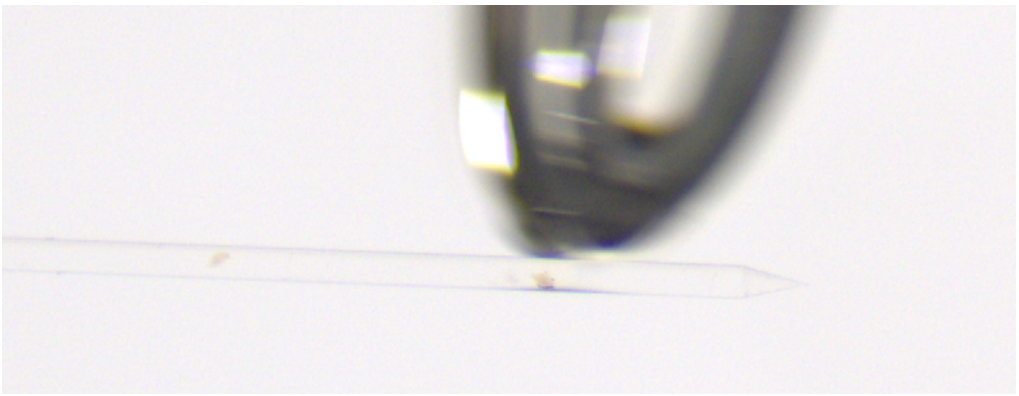

Figure 3.2: image of the fibre probe tip, with some fouling present, along with an out of focus bubble behind the probe.

3.3. Measurement limitations and requirements

The camera will store images inside the memory of the computer, and from there the images will be saved. Due to the write speed of the drive the memory usage of the computer will slowly increase, and once the memory is completely full frames will be dropped, this happens after around 2 minutes (120 seconds). The fibre probe software has a minimal amount of events somewhere around 380 events. If the number is lower than this the software will often crash when processing the measurement. In the ideal situation the amount of events would equal the event frequency multiplied by the maximum time the camera works without dropping frames. However preliminary measurements showed the event frequency for water to be around 3 Hz resulting in 360 events for this time frame, which is below the

threshold which still processes correctly. As the software still sometimes crashes even with a higher amount of events, the amount of events for a single measurement was chosen as 400 events for the water measurements, and 500 for the ethanol and NaCl measurements because a lower validity for these measurements is expected. This will ensure both measurement techniques will overlap as much as possible with each technique evenly spread over the entire time frame.

To ensure the proper function of the algorithm the settings of this algorithm were tested. Using a variant of the algorithm which showed all the processing steps with a 10% decrease (top row in fig 2.3) and increase (bottom row in fig 2.3) for the last performed processing step, the settings were tested. The settings contained the following values: Sobel filter threshold, kernel height and width, the maximum length of dark pixels at the image edge, minimal bubble size, and minimal area covered in the fitted ellipse. For the Sobel filter threshold a value of 0.15 was chosen at first, this however caused a lot of noise in certain images causing them to be filled in completely by the further processing steps and this was later adjusted to 0.3 which still yielded the actual bubbles but discarded enough of the noise to prevent complete filling of images. The bubbles were wider than they were high, and as such the elliptical kernel was wider than it was high as well. If the kernel was chosen too small, gaps in the edge could not be sufficiently filled, if it was chosen too large details in the curvature of the edge would be lost. A such a quite small kernel of 15 pixels high, and 30 pixels wide was chosen, which could fill small gaps sufficiently without too much loss of detail. The minimal size of an object which would still be seen as a bubble was chosen as 60000 pixels, this was to eliminate smaller objects caused by noise on the images which were small dust particles for example. Lastly a stretch of 100 pixels was chosen as the limit for closing small gaps at the edge, Most bubbles were larger than this so only small gaps caused by a lack of sharp edges at the edge of the image would be closed. Bubbles would not get connected by this process because they were further away from each other than 100 pixels (the closest bubbles being around 200 pixels apart). Lastly the amount of area inside the entire fitted ellipse covered by the bubble was used as a parameter for goodness-of-fit, at least 0.5 would be required to ensure that at least half of the bubble and fitted ellipse would be on the image, however testing images using a higher airflow showed some overlapping bubbles to pass this criterion as well with a fill level of up to 0.6. Even though overlapping bubbles weren't expected, as previously stated the expected distance was 200 pixels at least, the used value was set at 0.65, which would prevent overlapping bubbles to pass the filter as well as any very close bubbles connected through the edge closing process. Which resulted in the setting presented in table 3.1.

Setting	value
Sobel filter threshold	0.3
kernel height	15 pixels
kernel width	30 pixels
minimal area	60000 pixels
maximum edge stretch	100 pixels

Table 3.1: Caption

To determine the required amount of events for the fibre probe the relationship for the sample size (eq 2.4) was used with the standard deviation determined from a very large measurement the geometric mean of which was assumed as the true geometric mean. Plotting the mean for every added sample with the predicted amount of required samples for a specified fraction showed if the predicted required sample size aligned with the performed measurement. In water (fig 3.3) and with a maximum deviation factor (P) of 0.01 for the velocity and 0.02 for the diameter, the required amount of samples were found to be 1019 and 1115 respectively. The different values for P follow from a larger standard deviation for the diameter values.

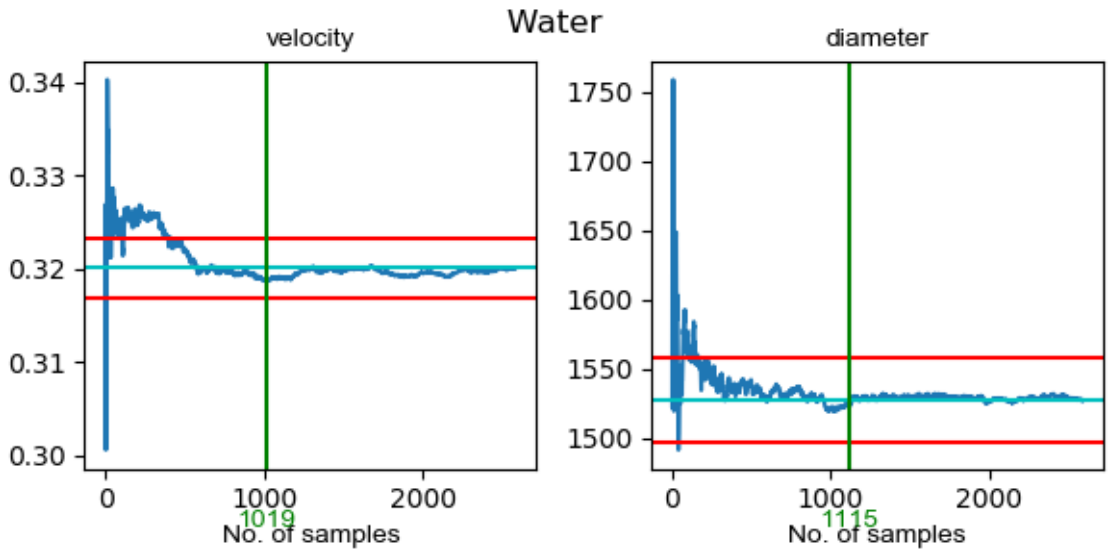

Figure 3.3: Evolution of the means (blue) for velocity (m/s)(left) and diameter (μm)(right) of fibre probe measurements in pure water. With the required amount of samples (green) to approach the assumed true geometric mean (cyan) within a specified maximum deviation factor, shown as lines above and below the mean (red).

For measurements in 100g/L ethanol water mixtures (fig 3.4) the same values for the maximum deviation factor were used. The required amount of samples were 894 for the velocity and 966 for the diameter of the bubbles.

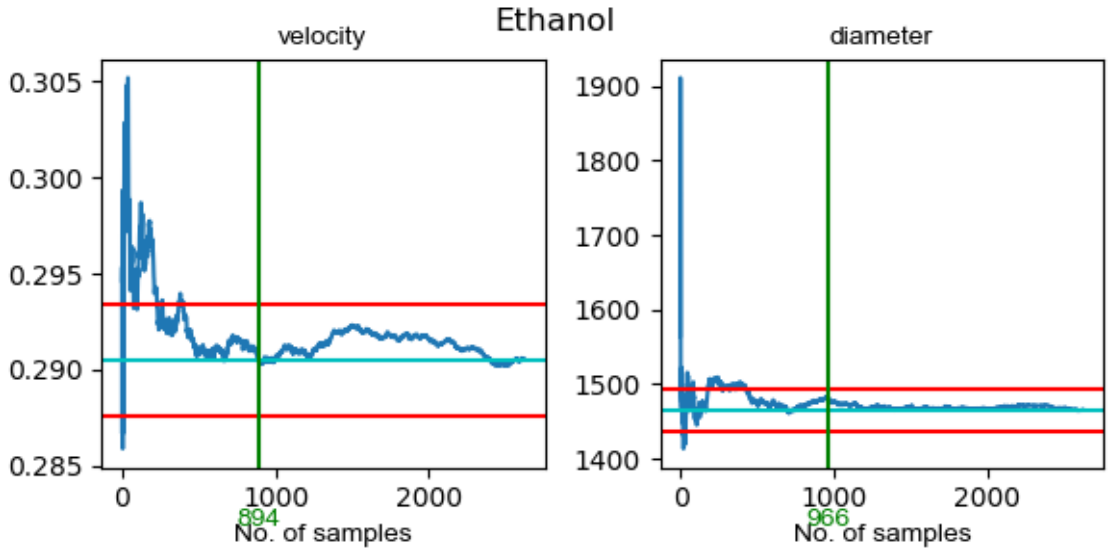

Figure 3.4: Evolution of the means (blue) for velocity (m/s)(left) and diameter (μm)(right) of fibre probe measurements in a 100 g/L ethanol water mixture. With the required amount of samples (green) to approach the assumed true geometric mean (cyan) within a specified maximum deviation factor, shown as lines above and below the mean (red).

For measurements in 0.4M NaCl dissolved in water, the first measurement was very inconsistent (fig 3.5). This was however due to fouling of the probe and after cleaning the probe this problem was alleviated. The required amount of samples (fig 3.6) were found as 1164 for the velocity and 1201 for the diameter. These deviation factors are quite restrictive, as such a sample number of at least 900 will be deemed sufficient. This lower sample number will increase the deviation factors only slightly.

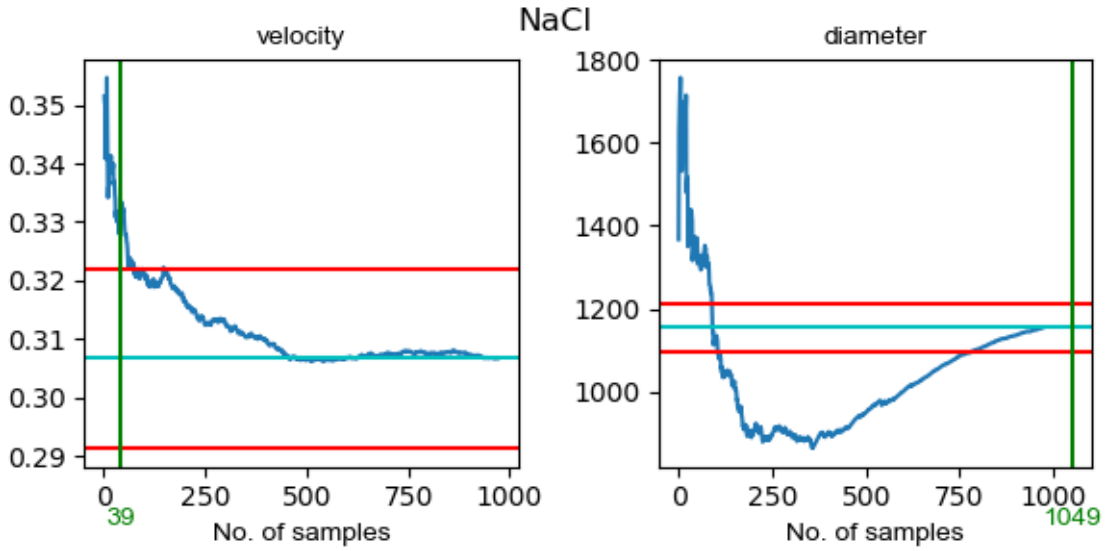

Figure 3.5: Incorrect evolution of the means (blue) for velocity (m/s)(left) and diameter (μm)(right) of fibre probe measurements in a 0.4M NaCl water mixture. With the required amount of samples (green) to approach the assumed true geometric mean (cyan) within a specified maximum deviation factor, shown as lines above and below the mean (red).

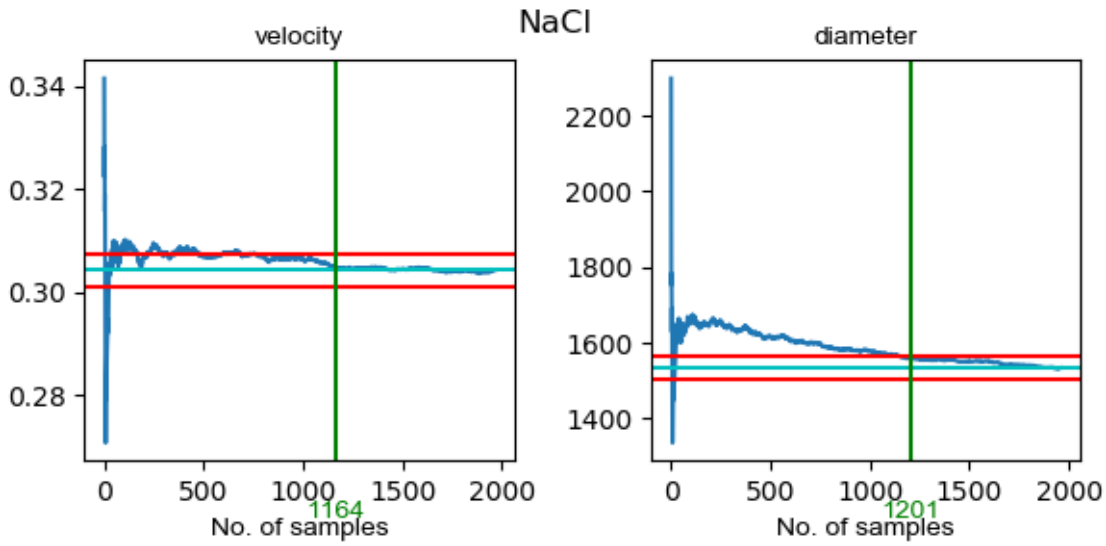

Figure 3.6: Evolution of the means (blue) for velocity (m/s)(left) and diameter (μm)(right) of fibre probe measurements in a 0.4M NaCl water mixture. With the required amount of samples (green) to approach the assumed true geometric mean (cyan) within a specified maximum deviation factor, shown as lines above and below the mean (red).

4

Results

4.1. General

All measurements showed a clear difference between the camera data and the probe data. By using a 1 sample KS-test it was found that none of the data sets were normally distributed, and only a few were log normally distributed. Because there were no pairs of normally distributed data sets no t-tests could be performed, as such only KS-tests were performed. These tests would show if the probe data and camera data share a distribution. All measurements were performed over the same time frame, however it could not be determined with certainty if all measured bubbles with both measurement techniques were exactly the same bubbles.

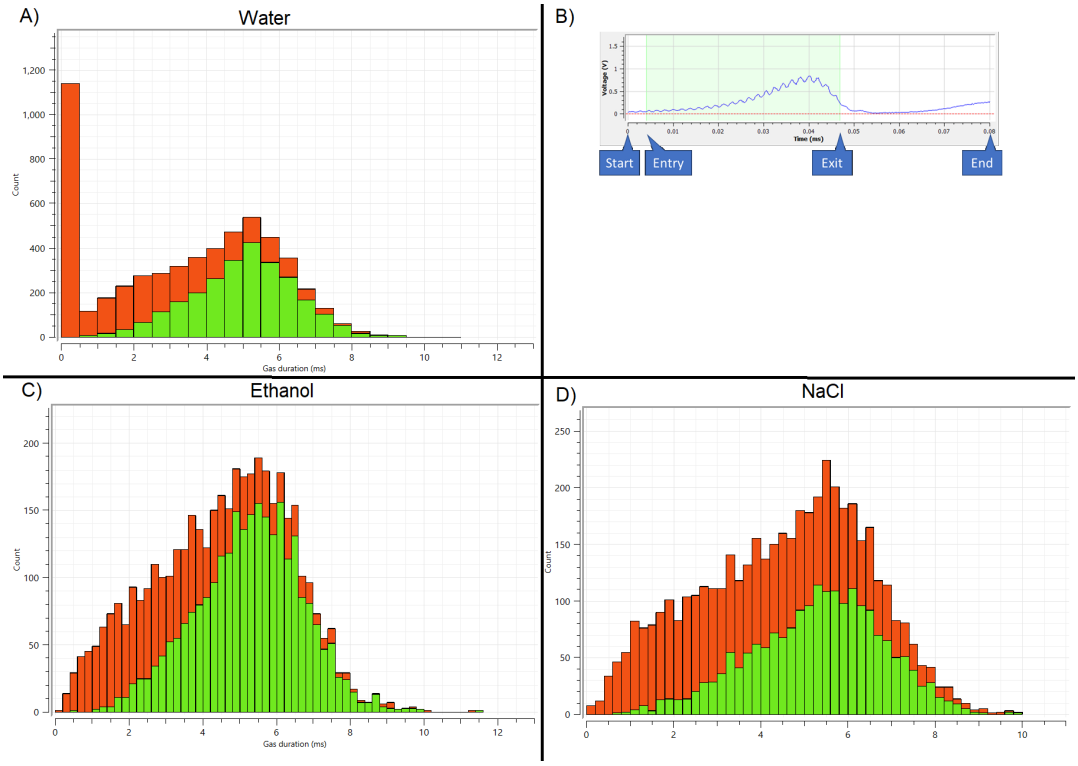

Figure 4.1: Gas duration histograms of three liquids (pure water, 100g/L ethanol mixture, and 0.4M NaCl) and the process signal of an incorrect bubble. Green bars show valid events, red bars invalid events. A) The histogram for pure water with a large number of very short duration bubbles. B) Signal measured by the probe for one such very short bubble, the end time shows the start of the actual longer bubble signal. C) The histogram for the ethanol mixture D) The histogram for NaCl.

For the probe measurements the validity of the events showed if the velocity could be calculated precisely enough. Because the speed of the invalid events was not known only the gas duration could be

compared. For the distribution in pure water (fig 4.1A) it was clear that there were a lot of short duration (below 0.5ms, either small or fast) bubbles. These short events were probably caused by vibrations in the bubbles causing a small "bubble" to appear just before the actual bubble approached the probe (fig 4.1B). This presumption was confirmed by the manufacturer of the probe. This fraction of short duration bubbles does not show up for both ethanol (fig 4.1C) and NaCl (fig 4.1D) mixtures where the spread of events was far more even across the different durations.

4.2. Water

To determine if a difference in measurements of the fibre probe and camera were due to the setup, measurements with pure water were performed. A total of 11263 bubbles were measured by the camera and processing algorithm and a total of 903 events were recorder by the probe. The distributions (fig 4.2) showed a very clear overlap for the velocity peaks, the diameter peaks had a distinct offset between the two techniques. The data sets from the probe both probably followed a log normal distribution as their p-values were greater than 0.05 (table 4.1), the distributions of the camera data did not follow such a distribution as their p-values were below 0.05 (table 4.1). To compare the different techniques the two sample KS-test showed neither the velocity or size data sets shared a distribution. The probe did show some faster bubbles above 0.4 m/s which the camera did not show. These missing bubbles could not be due to a limit in the camera, the camera should have been able to measure bubbles up to 5mm in size with a velocity up to 0.6m/s. The diameter as presented by the probe was a local height, and from the camera data the height of the bubbles at the line of the probe tip was used as a comparable data set. This was however probably not entirely comparable because the diameter distributions do not overlap. This could have been caused by the fact that this line was drawn over the entire image, and not more locally near the tip and if the tip caused a general drift more radially outward from the probe this would explain the difference. Another more likely explanation is the 3D nature of the bubbles whereas the image is a 2D projection of this object. As such the line intersecting the bubble on the image would always be the highest part on that slice of the bubble, where the fibre probe could pierce the bubble on a thinner part of the bubble. Lastly a comparison between the comparable diameter of the camera data, and the calculated equivalent diameter was performed (fig 4.3). This showed the equivalent diameter to be significantly lower, which can be explained by the fact that the bubbles more closely resembled flat discs than spheres.

Table 4.1: Statistical properties of the data sets gained from pure water.

		camera	probe
velocity	mean	0.308	0.316
	standard deviation	0.039	0.052
	normal p-value	0	0
	lognormal p-value	0	0.236
diameter	mean	1898.0	1589.8
	standard deviation	582.6	465.9
	normal p-value	0	0
	lognormal p-value	0	0.979

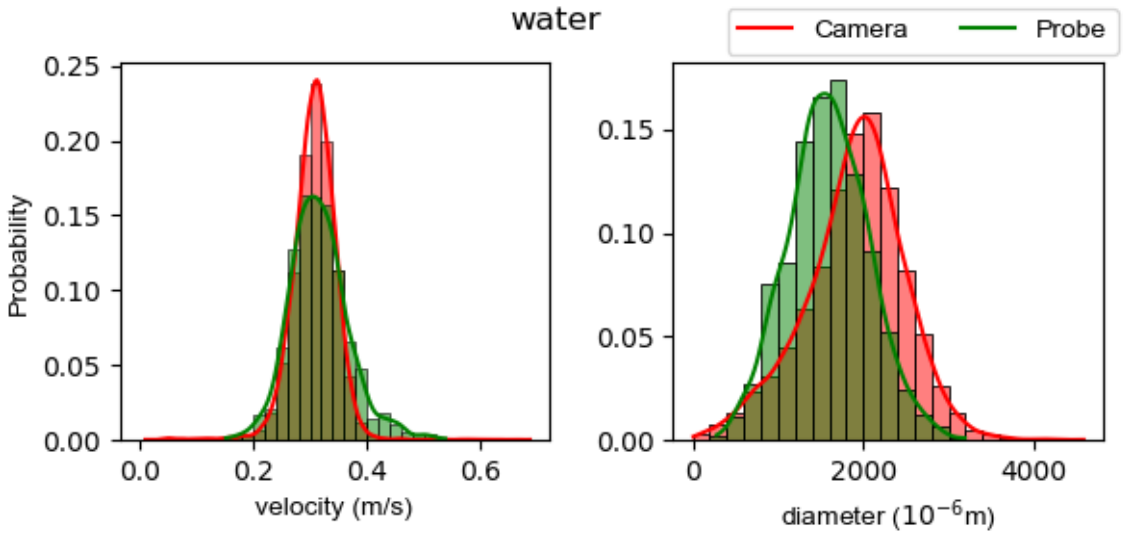

Figure 4.2: Distribution of the measurement data from the camera (red) and fibre probe (green), for both the velocity (left), and size(right). Measured in pure water.

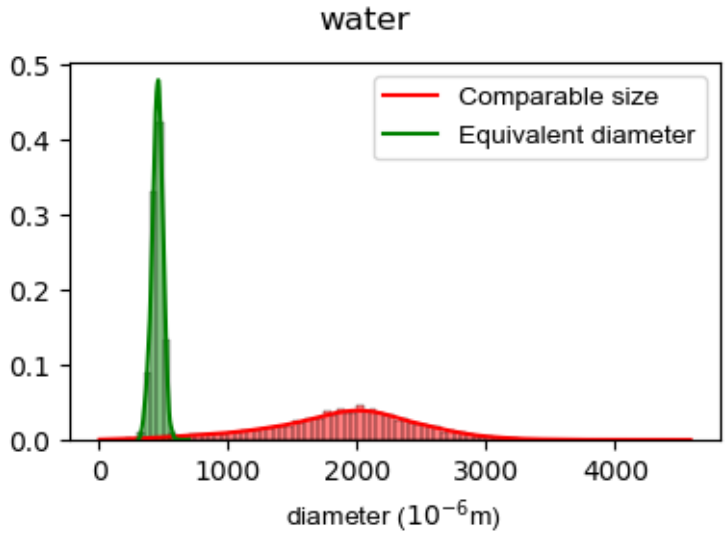

Figure 4.3: Comparison between the diameter used as comparable data to the fibre probe measurements, and the calculated equivalent diameter in water.

4.3. Ethanol

For the measurements with 100g/L ethanol, there were clear differences between the camera and probe data as shown by differences in the statistical properties of the data (table 4.2) and their distributions (fig 4.4). For the velocity distribution the probe data shows a wider spread which is reflected in the higher standard deviation. The mean of the values for the probe data is lower as compared to the camera. Performing the KS-test for the velocity distributions yields a p-value of 0 thus these data sets do not share a distribution. For the size (diameter) data there is a difference compared to the velocity data, the camera has a higher spread and standard deviation. The mean of the size from the camera data is however still larger than the mean from the probe data. For these data sets the p-value was 0 which again means these data sets do not share a distribution. For both bubble properties there is a clear difference between the distributions from each measuring method which might be caused by an error in the probe, there are however no clear limits where the probe doesn't detect any bubbles, where the

camera clearly does. The comparison between the equivalent diameter and the comparable diameter (fig 4.5) did not show any clear difference compared to the distributions for pure water. The shapes of these distributions made a proper comparison difficult.

Table 4.2: Statistical properties of the data sets gained from a 100g/L ethanol mixture.

		camera	probe
velocity	mean	0.299	0.293
	standard deviation	0.042	0.046
	normal p-value	0	0
	lognormal p-value	0	0.542
diameter	mean	1755.6	1560.2
	standard deviation	564.4	436.0
	normal p-value	0	0
	lognormal p-value	$7.08 * 10^{-13}$	$5.92 * 10^{-6}$

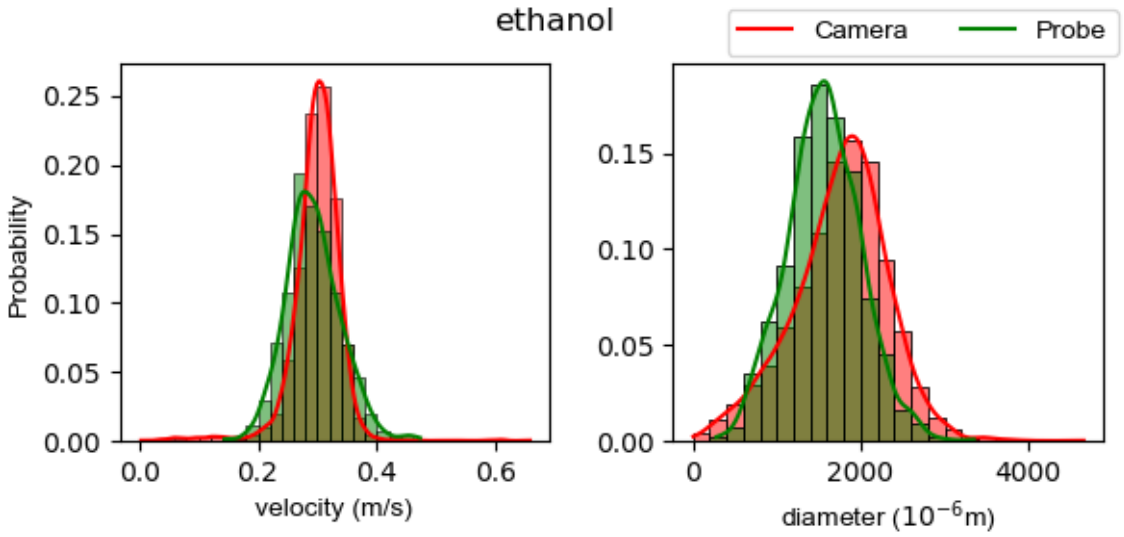

Figure 4.4: Distribution of the measurement data from the camera (red) and fibre probe (green), for both the velocity (left), and size(right). Measured in 100g/L ethanol.

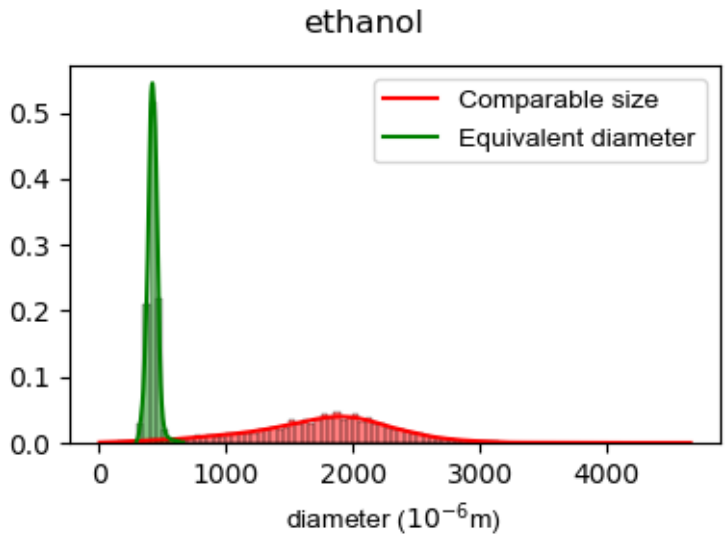

Figure 4.5: Comparison between the diameter used as comparable data to the fibre probe measurements, and the calculated equivalent diameter in a 100g/L ethanol mixture.

4.4. NaCl

For the measurements in a mixture of 0.4M NaCl The comparison between the probe and camera data sets showed only the velocity distribution for the probe data set to probably follow a log normal distribution. This was because only the p-value from the KS-test for this distribution was above 0.05 (table 4.3). Both size distributions showed a bend just before the peak (fig 4.6). This could indicate a shared distribution and a clear influence of the salt on the actual size distribution of the bubbles. However the data sets for both size and velocity did not share a distribution as the p-value for the two sample KS-tests were both 0. The comparison between the equivalent diameter and the comparable diameter (fig 4.7) showed the slight bent for the comparable data, but this wasn't visible in the equivalent diameter, this is probably due to the fact this distribution was very narrow.

Table 4.3: Statistical properties of the data sets gained from a 0.4M NaCl mixture.

		camera	probe
velocity	mean	0.316	0.305
	standard deviation	0.039	0.045
	normal p-value	0.0	0.0
	lognormal p-value	$1.41 * 10^{-4}$	0.546
diameter	mean	1815.3	1574.1
	standard deviation	628.2	461.1
	normal p-value	0	0
	lognormal p-value	0	0

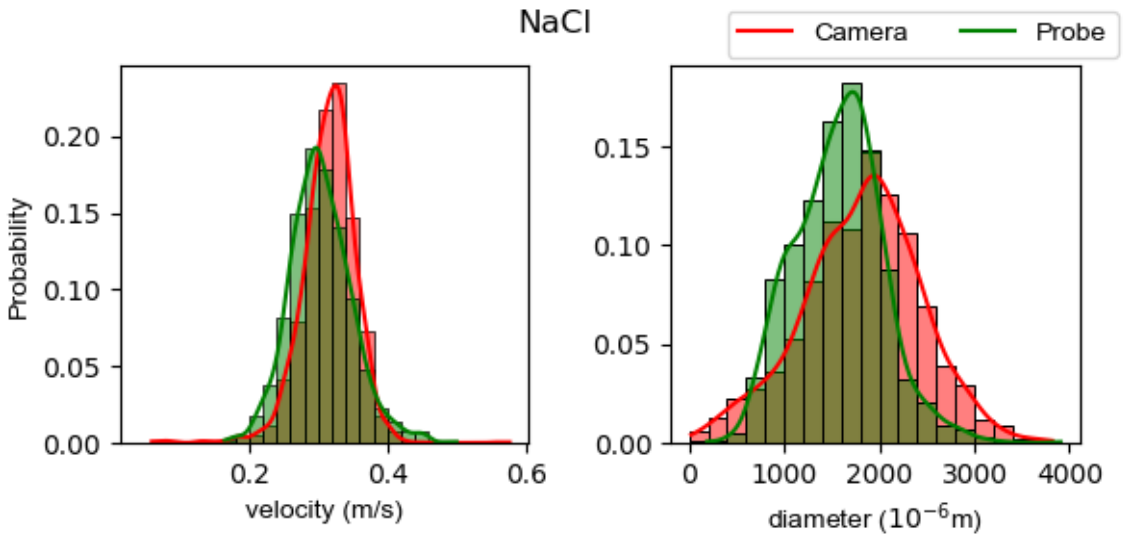

Figure 4.6: Distribution of the measurement data from the camera (red) and fibre probe (green), for both the velocity (left), and size(right). Measured in 0.4M NaCl

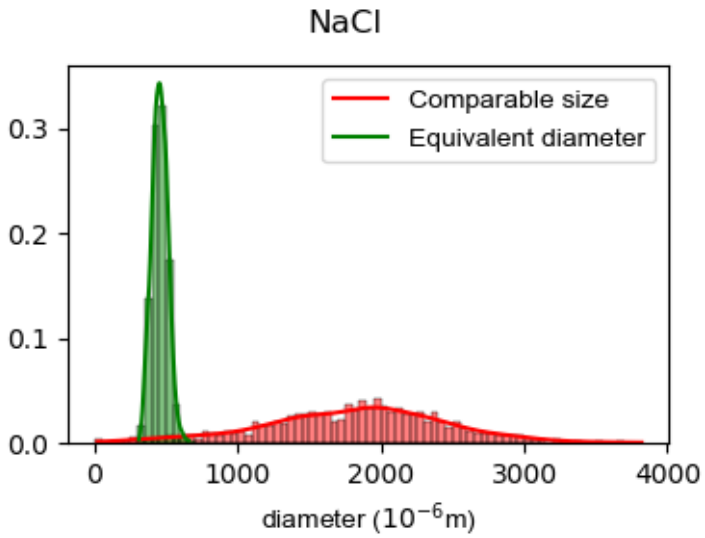

Figure 4.7: Comparison between the diameter used as comparable data to the fibre probe measurements, and the calculated equivalent diameter in a 0.4M NaCL solution.

5

Conclusions and Recommendations

For this report the aim was to gain insight into possible limits for determining bubble size and velocity using an optical fibre probe in liquids containing ethanol or NaCl. By using the data from the fibre probe with the data of a camera the distributions for both bubble size and velocity were determined. Pure water was used to compare the data output of both methods. For the bubble velocity in water it was determined that the camera data yielded a lower standard deviation compared to the probe data. This was true as well for ethanol and NaCl. These data sets did not follow a (log) normal distribution as was expected except for the data set measured by the probe in pure water. The means for both the camera and probe data were quite close for each liquid with the largest difference (0.011m/s) in the NaCl mixture which was only about a third of the standard deviations of these data sets. For the bubble size the camera data again showed a consistently larger standard deviation than the probe data. The difference between the means of the camera data and probe data was relatively larger, which was around half of the average standard deviations. The difference between the size distributions could most probably be attributed to an overestimation of the cross section near the fibre probe, which served as data which should be comparable with the probe data. The clearest difference between the pure water measurements and the measurements with added ethanol or NaCl was the distribution of invalid events as registered by the fibre probe. Sorting the events based on gas duration yielded a large peak for the shortest durations, these were found to be small signal spikes just before an actual bubble approached the fibre probe. This signal could have been caused by vibrations within the bubbles. This peak disappeared in both ethanol and NaCl experiments which could be explained by an increased rigidity of the bubbles causing them to vibrate less, but it was not possible to confirm this suspicion.

No clear limits in terms of size or velocity of bubbles were found for the fibre probe at the extreme concentrations used in these measurements. Because there was no clear cut off value below or above which the camera did clearly measure bubbles and the probe did not. A very clear relation between the data gained from the fibre probe and the camera was however not found due to the exact distributions to be unknown of most data sets, and as such a relation between the probe measurements and the equivalent diameter could not be established. To improve the overlap between the camera data an fibre probe data in pure water two improvements could be performed. A better estimation of comparable data from the camera to use with the fibre probe data might yield a conversion factor from the diameter as presented by the fibre probe to the equivalent diameter as determined by the camera. Secondly a more precise method of determining the bubble speed with a higher speed camera to prevent averaging the speed between frames could widen the distribution of camera velocities. If both velocity and size distributions would be equal or at least have the same shape a relation between these could be better established, which would allow more insight into the exact influence of the compounds added on the measurements of the fibre probe. Lastly changing the air inflow/sparger to create smaller or faster bubbles could better show a possible limit for the probe, as currently the camera did not measure very small or fast bubbles.

References

AG, B. (n.d.). *Basler ace acA1920-150uc - area scan camera* [Basler AG]. Retrieved April 24, 2023, from https://www.baslerweb.com/en/products/cameras/area-scan-cameras/ace/aca1920-150uc/

Augier, F., & Raimundo, P. M. (2021). Effect of rheology on mass transfer and bubble sizes in a bubble column operated in the heterogeneous regime. *The Canadian Journal of Chemical Engineering*, *99*(5), 1177–1185. https://doi.org/10.1002/cjce.23903

Bai, F. W., Anderson, W. A., & Moo-Young, M. (2008). Ethanol fermentation technologies from sugar and starch feedstocks. *Biotechnology Advances*, *26*(1), 89–105. https://doi.org/10.1016/j.biotechadv.2007.09.002

Bai, W., Deen, N. G., Mudde, R. F., & Kuipers, J. A. M. (n.d.). ACCURACY OF BUBBLE VELOCITY MEASUREMENT WITH a FOUR-POINT OPTICAL FIBRE PROBE.

Besagni, G., & Inzoli, F. (2016). Comprehensive experimental investigation of counter-current bubble column hydrodynamics: Holdup, flow regime transition, bubble size distributions and local flow properties. *Chemical Engineering Science*, *146*, 259–290. https://doi.org/10.1016/j.ces.2016.02.043

Christian. (2021, September 9). *Direct linear least squares fitting of an ellipse*. https://scipython.com/blog/direct-linear-least-squares-fitting-of-an-ellipse/

Colombet, D., Legendre, D., Cockx, A., Guiraud, P., Risso, F., Daniel, C., & Galinat, S. (2011). Experimental study of mass transfer in a dense bubble swarm. *Chemical Engineering Science*, *66*(14), 3432–3440. https://doi.org/10.1016/j.ces.2011.01.020

Firouzi, M., Howes, T., & Nguyen, A. V. (2015). A quantitative review of the transition salt concentration for inhibiting bubble coalescence. *Advances in Colloid and Interface Science*, *222*, 305–318. https://doi.org/10.1016/j.cis.2014.07.005

Garcia-Ochoa, F., & Gomez, E. (2009). Bioreactor scale-up and oxygen transfer rate in microbial processes: An overview. *Biotechnology Advances*, *27*(2), 153–176. https://doi.org/10.1016/j.biotechadv.2008.10.006

Hale, W. E. (1972). Sample size determination for the log-normal distribution. *Atmospheric Environment (1967)*, *6*(6), 419–422. https://doi.org/10.1016/0004-6981(72)90138-2

Keitel, G., & Onken, U. (1982). The effect of solutes on bubble size in air-water dispersions [Publisher: Taylor & Francis _eprint: https://doi.org/10.1080/00986448208911616]. *Chemical Engineering Communications*, *17*(1), 85–98. https://doi.org/10.1080/00986448208911616

Klasson, K. T., Ackerson, M. D., Clausen, E. C., & Gaddy, J. L. (1993). Biological conversion of coal and coal-derived synthesis gas. *Fuel*, *72*(12), 1673–1678. https://doi.org/10.1016/0016-2361(93)90354-5

Lefebvre, A., Mezui, Y., Obligado, M., Gluck, S., & Cartellier, A. (2022). A new, optimized doppler optical probe for phase detection, bubble velocity and size measurements: Investigation of a bubble column operated in the heterogeneous regime. *Chemical Engineering Science*, *250*, 117359. https://doi.org/10.1016/j.ces.2021.117359

Luong, J. H. T. (1985). Kinetics of ethanol inhibition in alcohol fermentation [_eprint]. *Biotechnology and Bioengineering*, *27*(3), 280–285. https://doi.org/10.1002/bit.260270311

McClure, D. D., Deligny, J., Kavanagh, J. M., Fletcher, D. F., & Barton, G. W. (2014). Impact of surfactant chemistry on bubble column systems. *Chemical Engineering & Technology*, *37*(4), 652–658. https://doi.org/10.1002/ceat.201300711

OpenCV: Morphological transformations. (n.d.). Retrieved June 22, 2023, from https://docs.opencv.org/4.x/d9/d61/tutorial_py_morphological_ops.html

Park, S. H., Park, C., Lee, J., & Lee, B. (2017). A simple parameterization for the rising velocity of bubbles in a liquid pool. *Nuclear Engineering and Technology*, *49*(4), 692–699. https://doi.org/10.1016/j.net.2016.12.006

Puiman, L., Abrahamson, B., Lans, R. G. J. M. v. d., Haringa, C., Noorman, H. J., & Picioreanu, C. (2022). Alleviating mass transfer limitations in industrial external-loop syngas-to-ethanol fermentation. *Chemical Engineering Science*, *259*, 117770. https://doi.org/10.1016/j.ces.2022.117770

Python code for bubble tracking. (n.d.). http://soft-matter.github.io/trackpy/v0.3.0/tutorial/custom-feature-detection.html

Villegas, L. R., Colombet, D., Guiraud, P., Legendre, D., Cazin, S., & Cockx, A. (2019). Image processing for the experimental investigation of dense dispersed flows: Application to bubbly flows. *International Journal of Multiphase Flow*, *111*, 16–30. https://doi.org/10.1016/j.ijmultiphaseflow.2018.10.017

Zhou, H., & Niu, X. (2020). An image processing algorithm for the measurement of multiphase bubbly flow using predictor-corrector method. *International Journal of Multiphase Flow*, *128*, 103277. https://doi.org/10.1016/j.ijmultiphaseflow.2020.103277